5280–5290 *Nucleic Acids Research, 2010, Vol. 38, No. 16* *Published online 29 April 2010*
doi:10.1093/nar/gkq304

Electron attachment-induced DNA single-strand breaks at the pyrimidine sites

Jiande Gu[1,2,*], Jing Wang[2] and Jerzy Leszczynski[2,*]

[1]Drug Design & Discovery Center, State Key Laboratory of Drug Research, Shanghai Institute of Materia Medica, Shanghai Institutes for Biological Sciences, CAS, Shanghai 201203 P. R. China and [2]Interdisciplinary Nanotoxicity Center, Department of Chemistry and Biochemistry, Jackson State University, Jackson, MS 39217, USA

Received March 2, 2010; Revised April 7, 2010; Accepted April 12, 2010

ABSTRACT

To elucidate the contribution of pyrimidine in DNA strand breaks caused by low-energy electrons (LEEs), theoretical investigations of the LEE attachment-induced $C_{3'}$–$O_{3'}$, and $C_{5'}$–$O_{5'}$ σ bond as well as *N*-glycosidic bond breaking of 2′-deoxycytidine-3′,5′-diphosphate and 2′-deoxythymidine-3′,5′-diphosphate were performed using the B3LYP/DZP++ approach. The base-centered radical anions are electronically stable enough to assure that either the C–O or glycosidic bond breaking processes might compete with the electron detachment and yield corresponding radical fragments and anions. In the gas phase, the computed glycosidic bond breaking activation energy (24.1 kcal/mol) excludes the base release pathway. The low-energy barrier for the $C_{3'}$–$O_{3'}$ σ bond cleavage process (∼6.0 kcal/mol for both cytidine and thymidine) suggests that this reaction pathway is the most favorable one as compared to other possible pathways. On the other hand, the relatively low activation energy barrier (∼14 kcal/mol) for the $C_{5'}$–$O_{5'}$ σ bond cleavage process indicates that this bond breaking pathway could be possible, especially when the incident electrons have relatively high energy (a few electronvolts). The presence of the polarizable medium greatly increases the activation energies of either C–O σ bond cleavage processes or the *N*-glycosidic bond breaking process. The only possible pathway that dominates the LEE-induced DNA single strands in the presence of the polarizable surroundings (such as in an aqueous solution) is the $C_{3'}$–$O_{3'}$ σ bond cleavage (the relatively low activation energy barrier, ∼13.4 kcal/mol, has been predicted through a polarizable continuum model investigation). The qualitative agreement between the ratio for the bond breaks of $C_{5'}$–$O_{5'}$, $C_{3'}$–$O_{3'}$ and *N*-glycosidic bonds observed in the experiment of oligonucleotide tetramer CGAT and the theoretical sequence of the bond breaking reaction pathways have been found. This consistency between the theoretical predictions and the experimental observations provides strong supportive evidences for the base-centered radical anion mechanism of the LEE-induced single-strand bond breaking around the pyrimidine sites of the DNA single strands.

INTRODUCTION

Both recent experimental and theoretical investigations of different DNA models have illustrated that low-energy electrons (LEE) play a vital role in the nascent stage of DNA radiolysis and may induce strand breaks in DNA via dissociative electron attachment (1–23). A comprehensive understanding of such LEE-induced DNA damages is one of the key steps towards governing the effects of ionizing radiation at a molecular level.

Theoretical investigations on the mechanism of the LEE-induced DNA have been mainly focused on the pyrimidine families of DNA fragments (6,13,16,18,21,23). Based on the density functional theory (DFT) studies of the sugar–phosphate–sugar model, Li, Sevilla and Sanche (6) proposed that the near 0 eV electron may be captured first by the phosphate group, forming a phosphate-centered radical anion. More detailed study suggested that the excess electron is trapped in the dipolar field of two OH groups in the sugar–phosphate backbone (24). The subsequent $C_{3'}$–$O_{3'}$ or $C_{5'}$–$O_{5'}$ σ

*To whom correspondence should be addressed. Jiande Gu. Tel: +86 21 5080 6720; Fax: +86 21 5080 7088; Email: jiandegush@go.com
Correspondence may also be addressed to Jerzy Leszczynski. Tel: +1 601 979 3482; Fax: +1 601 979 7823; Email: jerzy@icnanotox.org

bond breaking was estimated to have an energy barrier of ~10 kcal/mol. Other theoretical studies (10) suggested that electrons with kinetic energies near 0 eV cannot directly attach to the phosphate units at a significant rate. The small values of electron affinity [−0.003 and 0.033 eV (6)] of the evaluated sugar–phosphate–sugar model seem to suggest that, instead of the phosphate group in DNA species, LEEs might be trapped in the pyrimidine bases [with electron affinities of near 0 eV in experiments (25), and 0.03 eV (cytosine) and ~0.2 eV (thymidine) at the B3LYP/DZP++ level of theory (26)]. Recent experimental and theoretical investigations of the base-releasing process of pyrimidine nucleosides (8,13,16,18,21) have suggested that at the nascent stage, the excess electron resides on the π* orbital of pyrimidine in the radical anion, forming an electronically stable radical anion. The subsequent bond breaking might happen at either the C–O σ bond or *N*-glycosidic bond.

Based on the studies of different models [2′-deoxycytidine-3′-monophosphate and 2′-deoxythymidine3′-monophosphate molecule; (9–12,19)], Simons suggested that only in an aqueous solution, the very LEEs can attach to the π* orbitals of the DNA bases and then undergo $C_{3'}$–$O_{3'}$ bond cleavage (9,11,12,19). Negative electron affinities of the pyrimidine nucleotides in the gas phase, predicted in their studies, prevent the electron attachment to the bases. However, this conclusion does not agree with the experimental gas-phase investigations The negative values for electron affinity of the pyrimidine nucleotides in the gas phase (9–11) are contrary to the experimental results on DNA (24) and RNA (4) fragments. Both experiments and other higher level theoretical investigations provide definitely the positive electron affinities for the pyrimidine bases, the nucleosides, and the nucleotides in the gas phase (13,26–28). Moreover, experiments on DNA strand breaks induced by 0–4 eV electrons suggest that the strand breaks are initiated by electron attachment to the bases in the condensed phase (29). Other studies suggested that the excited states might play an important role in LEE-induced strand breaks in DNA in aqueous solutions (30,31).

The density functional theory investigations of LEE-induced C–O σ bond breaking of pyrimidine nucleotides based on various pyrimidine-monophosphate models (16,18,23) concluded that the mechanism of the LEE-induced single-strand bond breaking in DNA involves the attachment of an electron to the pyrimidine bases of DNA and the formation of base-centered radical anions even in the gas phase. These radical anions might subsequently undergo either C–O or glycosidic bond breaking, yielding neutral ribose radical fragments and the corresponding phosphoric anions or base anions. The $C_{3'}$–$O_{3'}$ bond cleavage is expected to dominate because of its low activation energy.

The elegantly selected models in the previous reaction pathway studies of LEE-induced DNA strand breaking have covered the main components of the DNA strands. It should be noted that in these studies three different bond ruptures have been investigated separately based on different models. The influences of the neighboring fragments on the bond breaking process have been neglected. For instance, phosphate group at 5′-position has not been taken into consideration in the models for the studies of the $C_{3'}$–$O_{3'}$ or *N*-glycosidic bond breaking. However, recent experiment demonstrates that the terminal phosphates affect significantly the LEE-induced strand breakages of DNA oligomers (32). Moreover, theoretical investigation on the electron attachment to the nucleoside-3′,5′-diphosphate suggests considerable influences of the phosphate group on the electron affinities (33). Therefore, a more complex model containing phosphate groups at both 3′- and 5′-positions of nucleoside is necessary for a more realistic elucidation of the mechanism of the damage at the pyrimidine sites in the DNA single strand by LEEs.

We report the first study of the reaction pathways of the LEE-induced pyrimidine-related DNA bond breakings of 2′-deoxycytidine-3′,5′-diphosphate (3′,5′-dCDP) and 2′-deoxythymidine-3′,5′-diphosphate (3′,5′-dTDP). Such a model allows simultaneous examination of both $C_{5'}$–$O_{5'}$ and $C_{3'}$–$O_{3'}$ bond cleavages and *N*-glycosidic bond rupture processes. (For a better description of the influence of the 3′-5′ phosphodiester linkage in DNA, and to avoid the unrealistic intramolecular proton transfer from the phosphate group at the 5′-position to the base, the $–OPO_3H$ moiety was terminated with CH_3 group; Figure 1). This conformation complements and enhances the previous studies of the monophosphate ester of the 2′-deoxyribonucleosides of pyrimidines, and provides information directly related to the important building blocks of DNA. In living systems, the phosphates of the nucleotides could be either negatively charged or neutralized by counterions. The neutral phosphate models used in this study represent situation in which counterions are closely bound to the phosphate group of DNA. However, the finding in the previous study (34) that the electron affinities of the nucleotides are independent of the counterions in aqueous solutions ensures the existence of electronically stable base-centered radical anions of nucleotides and provides support for the currently considered models.

METHOD OF CALCULATION

The DFT method employing B3LYP functional (35,36) with basis sets of double-ζ quality augmented by polarization and diffuse functions (denoted DZP++) was used to obtain optimized geometries, energetics and natural charges for the DNA subunits in both neutral and anionic forms. The DZP++ basis sets were constructed by augmenting the Huzinaga–Dunning (37–39) set of contracted double-ζ Gaussian functions. To complete the DZP++ basis, one even-tempered diffuse *s* function was added to each H atom, while sets of even-tempered diffuse *s* and *p* functions were centered on each heavy atom. The even-tempered orbital exponents were determined according to the recommendation of Lee and Schaefer (40).

The B3LYP functional has successfully reproduced the experimentally derived electron affinities of nucleobases

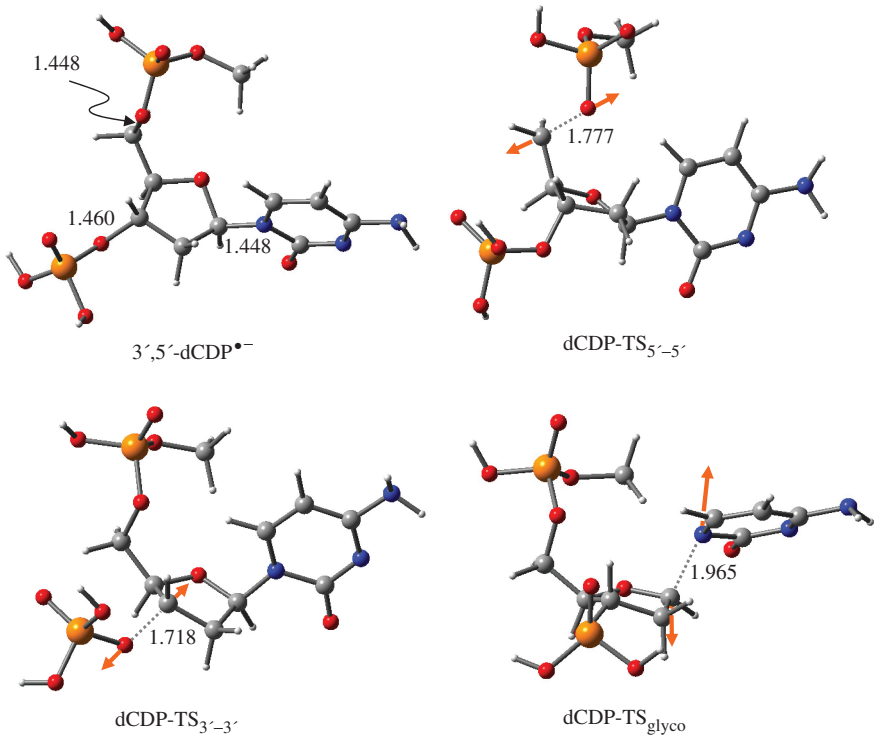

Figure 1. The optimized structures of the radical anion of 3′,5′-dCDP$^{\bullet-}$ and the transition state structures of the $C_{5'}$–$O_{5'}$ bond breaking (dCDT-$TS_{5'-5'}$), $C_{3'}$–$O_{3'}$ bond breaking (dCDT-$TS_{3'-3'}$) and *N*-glycosidic bond breaking (dCDT-TSglyco). Atomic distances are in angstrom. Orange arrows in the transition states represent the single imaginary frequency related vibration mode. Color representations: red for oxygen, gray for carbon, blue for nitrogen, orange for phosphorous and white for hydrogen.

(26,41) and also had accurately predicted the electron affinities of other DNA subunits such as nucleosides (27), which have been confirmed later by experiments (42). In addition, this functional provides a reliable description of the properties of the radical anions of the nucleotides and the reasonable determination of the activation energy barrier of the corresponding bond rupture (16,18,21,23). In accord with these previous successful applications, the B3LYP/DZP++ level of theory was also used in the present study.

To evaluate the potential energy surfaces of bond ruptures of DNA single strands in aqueous solution, a polarizable continuum model [PCM; (43)] with dielectric constant of water ($\varepsilon = 78.39$) was used to simulate the solvated environment of an aqueous solution. It should be noted that this PCM model approximate the real situation of aqueous solvation only to some extent, because the important effects of the microsolvation could not be included in this approach. Rather, the PCM model used in the present study accounts for the existence of the polarizable surroundings, which resembles situations in the experiment of LEE-induced bond breaks in the thin solid films. Natural Population Analysis was carried out using the mentioned functional and the DZP++ basis set with the Natural Bond Orbital analysis of Reed and Weinhold (44,45). The Gaussian 03 (46) system of DFT programs (Revision E. 01, 2004; Gaussian, Wallingford, CT, USA) was used for all computations.

Table 1. Electron attachment and detachment energies (in eV)

Process	EA_{ad}	VEA[a]	VDE[b]
3′,5′-dCDP → 3′,5′-dCDP$^{\bullet-}$ gas phase	0.27 (0.44)[c]	0.03[c]	0.71[c]
3′,5′-dTDP → 3′,5′-dTDP$^{\bullet-}$ gas phase	0.35 (0.52)[c]	0.17[c]	0.67[c]
3′,5′-dCDP → 3′,5′-dCDP$^{\bullet-}$ PCM model	1.99[c]	1.45	2.22
3′,5′-dTDP → 3′,5′-dTDP$^{\bullet-}$ PCM model	1.98[c]	1.57	2.17

Numbers within the parentheses are the zero-point vibrational energy corrected.
[a]VEA = E(neutral) − E(anion); the energies are evaluated using the optimized neutral structures.
[b]VDE = E(neutral) − E(anion); the energies are evaluated using the optimized anion structures.
[c]Gu *et al.* (33).

RESULTS AND DISCUSSION

Electron affinities of the nucleotides

The electron attachment and detachment energies of 3′,5′-dTDP and 3′,5′-dCDP are listed in the Table 1. These values are the same as those reported in the previous work (30). The adiabatic electron affinity (EA_{ad}) of 0.27 eV for 3′,5′-dCDP and 0.35 eV for 3′,5′-dTDP favor the formation of the corresponding radical anions. Meanwhile, the large values of the vertical detachment energy (VDE) for these two radical anions (0.71 eV for 3′,5′-dCDP$^{\bullet-}$ and 0.67 eV for 3′,5′-dTDP$^{\bullet-}$) ensure that, in the gas phase, electron detachment will not compete with the subsequent reactions

with the activation energy barrier <16.37 kcal/mol (0.71 eV) for 3′,5′-dCDP$^{\bullet-}$ and <15.45 kcal/mol (0.67 eV) for 3′,5′-dTDP$^{\bullet-}$.

Solvent effects remarkably increase the electron capturing ability of the nucleoside diphosphates. The EA_{ad}s are 1.99 eV and 1.98 eV for 3′,5′-dCDP$^{\bullet-}$ and 3′,5′-dTDP,$^{\bullet-}$ respectively, in the PCM calculation. Moreover, the increased VDE of 3′,5′-dCDP$^{\bullet-}$ (2.22 eV) and 3′,5′-dCTP$^{\bullet-}$ (2.17 eV) suggests that in aqueous solution the reactions with energy barrier less than 50 kcal/mol might undergo without electron detachment from these radical anion.

Activation energies of the $C_{5'}$–$O_{5'}$ σ bond breaking

The transition state structures for the $C_{5'}$–$O_{5'}$ σ bond cleavage process of the 3′,5′-dCDP$^{\bullet-}$ and 3′,5′-dTDP$^{\bullet-}$ have been located on the potential energy surface. These transition states are characterized by the existence of single imaginary vibrational frequency (934 i/cm for 3′,5′-dCDP$^{\bullet-}$ and 956 i/cm for 3′,5′-dTDP$^{\bullet-}$). The $C_{5'}$–$O_{5'}$ σ bond breaking can be documented by the elongated $C_{5'}$–$O_{5'}$ atomic distance of 1.777 Å for cytidine (1.769 Å for thymidine) and by the analysis of normal mode corresponding to the imaginary vibrational frequency (Figures 1 and 2). The activation energy of the $C_{5'}$–$O_{5'}$ σ bond cleavage process has been predicted to be 14.17 kcal/mol for 3′,5′-dCDP$^{\bullet-}$ and 13.37 kcal/mol for 3′,5′-dTDP$^{\bullet-}$ [Table 2; without the zero point energy (ZPE) correction]. These values are very close to the activation energy needed for the $C_{5'}$–$O_{5'}$ σ bond breaking in 5′-dCMPH$^{\bullet-}$ (14.27 kcal/mol) and in 5′-dTMPH$^{\bullet-}$ (13.84 kcal/mol) (16). Table 2 also lists the ZPE-corrected activation energy barriers and the corresponding free-energy differences at 298 K. Since these values are close to the activation energy barriers without the ZPE correction (within 2 kcal/mol), the following discussions will mainly be based on the results without the ZPE correction.

The solvent effects increase the $C_{5'}$–$O_{5'}$ σ bond breaking energy barrier dramatically. The energy barriers predicted using the PCM model are 18.73 kcal/mol for 3′,5′-dCDP$^{\bullet-}$ and 18.76 kcal/mol for 3′,5′-dTDP$^{\bullet-}$ (Table 3). This noticeable increase of the energy barrier is close to that found for the pyrimidine monophosphate models (17.97 kcal/mol for 5′-dCMPH$^{\bullet-}$ and 17.86 kcal/mol for 5′-dTMPH$^{\bullet-}$) in the presence of polarizable medium (16).

Activation energies of the $C_{3'}$–$O_{3'}$ σ bond breaking

The transition states for $C_{3'}$–$O_{3'}$ σ bond cleavage process in the radical anion of 3′,5′-dCDP and 3′,5′-dTDP are characterized by the elongated $C_{3'}$–$O_{3'}$ atomic distance (1.738 Å) and the normal mode (with the $C_{3'}$–$O_{3'}$ σ bond breaking pattern; Figures 1 and 2) corresponding to the imaginary vibrational frequency. The activation energy of the $C_{3'}$–$O_{3'}$ σ bond breaking has been predicted to be 6.02 and 6.37 kcal/mol for the radical anions (Table 2; without ZPE). This energy barrier is similar to that reported based on the 3′-dCMP and 3′-dTMP models (6.17 kcal/mol for the former and 7.06 kcal/mol for the latter) at the same level of theory (18). The presence of the phosphate group

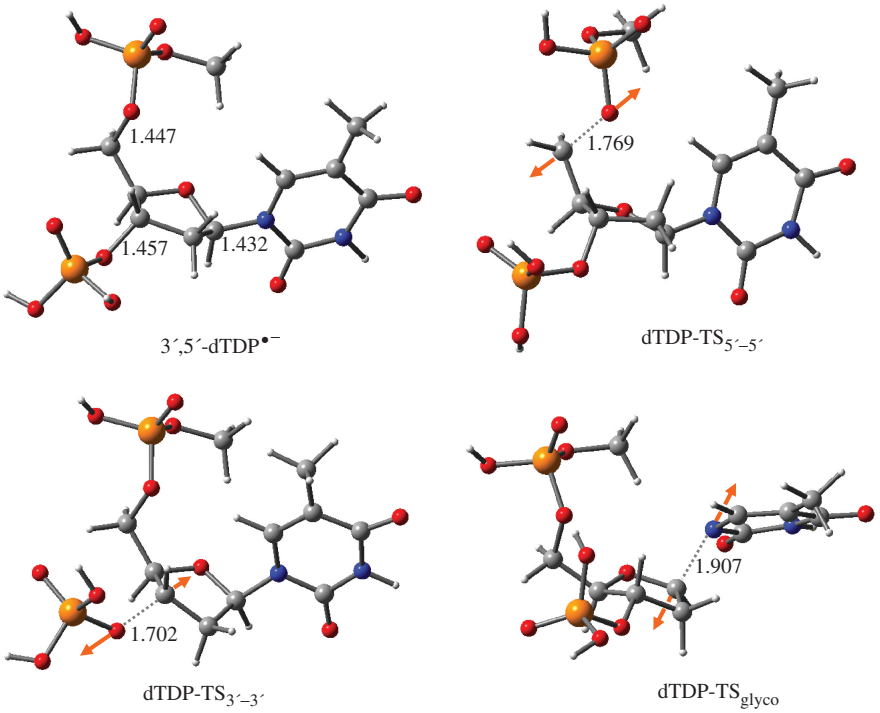

Figure 2. The optimized structures of the radical anion of 3′,5′-dTDP$^{\bullet-}$ and the transition state structures of the $C_{5'}$–$O_{5'}$ bond breaking (dTDP-$TS_{5'-5'}$), $C_{3'}$–$O_{3'}$ bond breaking (dTDP-$TS_{3'-3'}$) and *N*-glycosidic bond breaking (dTDP-TSglyco). Atomic distances are in angstrom. Orange arrows in the transition states represent the single imaginary frequency related vibration mode. Color representations: red for oxygen, gray for carbon, blue for nitrogen, orange for phosphorous and white for hydrogen.

Table 2. The relative energies of the transition states of bond break pathways in gas phase (kcal/mol)

Bond breaking	ΔE_{TS}[a]	$\Delta E^0{}_{TS}$[b]	$\Delta G^0{}_{TS}$[c]
3′,5′-dCDP$^{\bullet-}$			
$C_{5'}$–$O_{5'}$ bond	14.17 (14.27)[d]	12.31 (12.52)[d]	13.53 (12.75)[d]
$C_{3'}$–$O_{3'}$ bond	6.03 (6.17)[e]	5.23 (4.68)[e]	7.60 (4.54)[e]
N-glycosidic bond	26.21 (21.6)[f]	24.95 (20.4)[f]	26.57 (21.2)[f]
3′,5′-dTDP$^{\bullet-}$			
$C_{5'}$–$O_{5'}$ bond	13.39 (13.84)[d]	11.59 (11.91)[d]	11.49 (11.82)[d]
$C_{3'}$–$O_{3'}$ bond	6.04 (7.06)[e]	5.66 (5.29)[e]	6.92 (4.42)[e]
N-glycosidic bond	19.19 (18.9)[f]	18.79 (17.6)[f]	21.10 (18.0)[f]

[a]ΔE_{TS} = E(Transition state) – E(Radical anion).
[b]With the zero point energy (ZPE) correction.
[c]Free energy at T = 298 K.
[d]Using 2′-deoxypyrimidine-5′-monophosphate as the model (16).
[e]Using 2′-deoxypyrimidine-3′-monophosphate as the model (18).
[f]Using 2′-deoxypyrimidine nucleoside as the model (13).

Table 3. The relative energies of transition states of bond break pathways in aqueous solutions (kcal/mol)

Bond breaking process	ΔE_{TS}[a]
3′,5′-dCDP$^{\bullet-}$	
$C_{5'}$–$O_{5'}$ bond	18.73 (17.97)[b]
$C_{3'}$–$O_{3'}$ bond	13.36 (12.82)[c]
N-glycosidic bond	26.34
3′,5′-dTDP$^{\bullet-}$	
$C_{5'}$–$O_{5'}$ bond	18.76 (17.86)[b]
$C_{3'}$–$O_{3'}$ bond	14.18 (13.73)[c]
N-glycosidic bond	28.77

[a]ΔE_{TS} = E(Transition state) – E(Radical anion); using PCM model with ε = 78.39
[b]Using 2′-deoxypyrimidine-5′-monophosphate as the model (16).
[c]Using 2′-deoxypyrimidine-3′-monophosphate as the model (18).

at the 5′-position slightly decreases the $C_{3'}$–$O_{3'}$ σ bond breaking energy barrier.

The solvent effects increase the energy barrier of the $C_{3'}$–$O_{3'}$ σ bond rupture. The corresponding energy barrier in the PCM model is high up to 13.36 and 14.18 kcal/mol for 3′,5′-dCDP$^{\bullet-}$ and 3′,5′-dTDP$^{\bullet-}$, respectively (Table 3). In comparison, the energy barrier is 12.82 kcal/mol for 3′-dCMP$^{\bullet-}$ and 13.83 kcal/mol for 3′-dTMP$^{\bullet-}$ in the PCM model computations (18). It should be noted that these high activation energy barriers calculated based on the PCM model are close to that for the $C_{5'}$–$O_{5'}$ σ bond breaking process in the gas phase. Therefore, bimolecular nucleophilic substitution (SN2)-like mechanism observed in the gas phase for the $C_{3'}$–$O_{3'}$ σ bond breaking reaction is blocked by the solvent–solute interactions.

Activation energies of the *N*-glycosidic bond breaking

The transition state for *N*-glycosidic bond breaking of the radical anion has been located and characterized by the elongated $C_{1'}$–N_1 atomic distance (1.873 Å for 3′,5′-dCDP and 1.873 Å for 3′,5′-dTDP). This is further confirmed by the existence of a single imaginary vibrational frequency of 576 i/cm for 3′,5′-dTDP$^{\bullet-}$ and 500 i/cm for 3′,5′-dCDP$^{\bullet-}$ and the corresponding normal mode representing the $C_{1'}$–N_1 σ bond breaking (Figures 1 and 2). The activation energy of the $C_{1'}$–N_1 glycosidic bond breaking has been predicted to be 26.21 kcal/mol (Table 2; without ZPE) for 3′,5′-dCDP$^{\bullet-}$, ~4.61 kcal/mol higher than that found for the nucleoside model. An important feature in the glycosidic bond breaking structure representing transition state of cytidine is the existence of a strong H-bonding interaction between the proton at the $O_{5'}$ and the N_1 atom [the $H(O_{5'})\cdots N_1$ distance is 1.78 Å in dC$^{\bullet-}$). However, because of the phosphorylation at the $O_{5'}$ position in 3′,5′-dCDP$^{\bullet-}$, this H-bonding pattern is absent in the corresponding transition state. Therefore, this energy barrier increase is not unexpected. Similarly, in spite of the intramolecular H-bonding between the $O_{5'}$ atom and the proton of the 3′-phosphate, the activation energy for the *N*-glycosidic bond breaking in 3′,5′-dTDP$^{\bullet-}$ is also higher than that in the corresponding nucleoside [19.20 kcal/mol versus 18.9 kcal/mol; (13,21)]. This activation energy barrier increase for the *N*-glycosidic bond dissociation due to the presence of the adjoining phosphate groups corresponds to the recent experimental observation that while the LEE-induced base release percentage amounts to 16.5 in the oligomer TpT, it is reduced to 0.5 in the oligonucleotide pTpTp (32).

Similar to the discussed C–O σ bond rupture, the solvent effects raise the energy barrier of the *N*-glycosidic bond breaking. It is 28.77 kcal/mol for 3′,5′-dTDP$^{\bullet-}$ in the PCM model-simulated aqueous solutions. This substantial increase in the energy barrier due to the solvent–solute interactions is in accordance with the largely reduced dipole moment of the corresponding transition state (17.7 Debye versus 22.8 Debye for the optimized radical anion, without vibrational excitation) in aqueous solutions. On the other hand, the solvent–solute interactions only slightly increase the activation energy of the *N*-glycosidic bond rupture in 3′,5′-dCDP$^{\bullet-}$ (26.34 kcal/mol). Correspondingly, the dipole moments of the local minimum structure and the transition state of 3′,5′-dCDP$^{\bullet-}$ are very similar (17.9 Debye versus 17.0 Debye).

Products of the C–O σ and *N*-glycosidic bond breaking

Both $C_{3'}$–$O_{3'}$ and $C_{5'}$–$O_{5'}$ σ bond ruptures lead to the energetically stable complexes consisting of a phosphate anion and a corresponding carbon-centered neutral radical (Figure 3). In the case of the $C_{5'}$–$O_{5'}$ σ bond breaking, the products are 22.0 and 32.9 kcal/mol more stable than 3′,5′-dCDP$^{\bullet-}$ and 3′,5′-dTDP$^{\bullet-}$, respectively (Table 4). Meanwhile, the energies of the $C_{3'}$–$O_{3'}$ σ bond-broken products are 42.0 and 43.1 kcal/mol lower than those of the corresponding reactants, 3′,5′-dCDP$^{\bullet-}$ and 3′,5′-dTDP$^{\bullet-}$, respectively. The formation of a H-bond between the phosphate groups in the $C_{5'}$–$O_{5'}$ σ bond-broken product of 3′,5′-dTDP$^{\bullet-}$ and in the $C_{3'}$–$O_{3'}$ σ bond-broken products of both radical anions accounts for large energy decrease of these C–O σ bond-broken products. It should be noted that the strong H-bond in the $C_{3'}$–$O_{3'}$ σ bond-broken products includes the neutralizing hydrogen of the phosphate

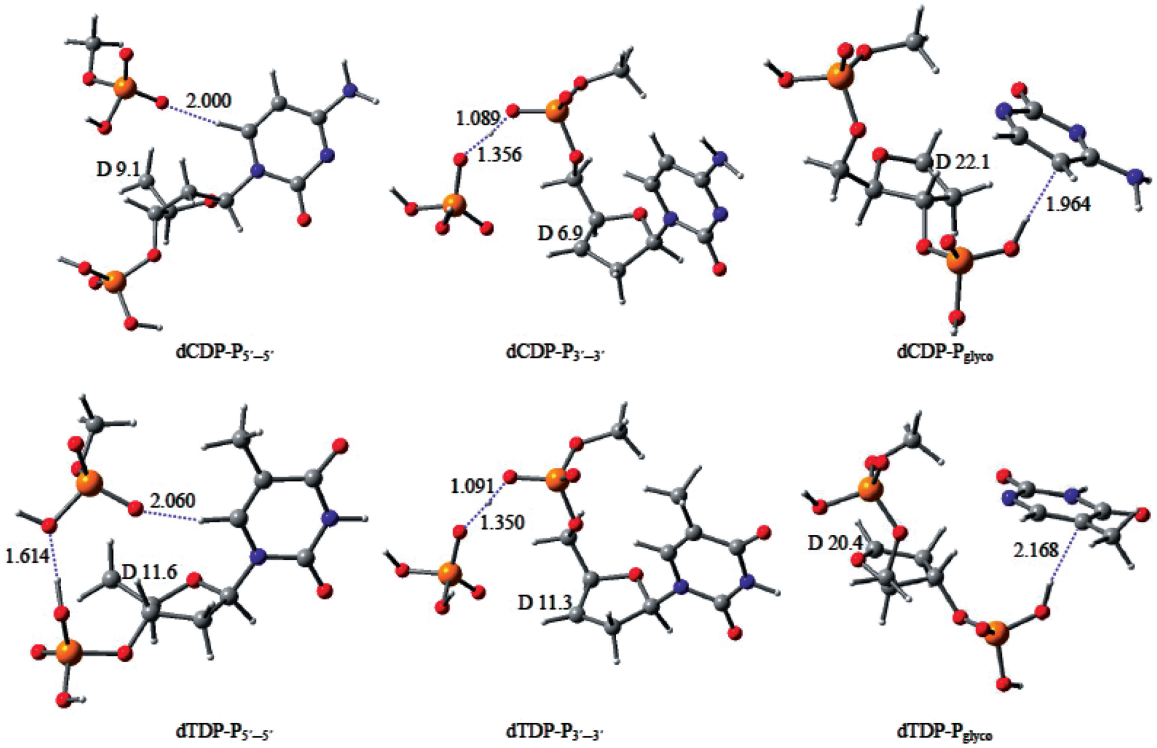

Figure 3. The optimized structures of the bond-broken product: $C_{5'}$–$O_{5'}$ (dCDP-$P_{5'-5'}$ and dTDP-$P_{5'-5'}$), $C_{3'}$–$O_{3'}$ (dCDP-$P_{3'-3'}$ and dTDP-$P_{3'-3'}$) and *N*-glycosidic (dCDP-P_{glyco} and dTDP-P_{glyco}) bond-broken products.

Table 4. The relative energies of the bond-broken products (kcal/mol)

Bond breaking process	ΔE[a]	ΔE_{PCM}[b]
3′,5′-dCDP$^{\bullet-}$		
$C_{5'}$–$O_{5'}$ bond	−22.00	−16.99
$C_{3'}$–$O_{3'}$ bond	−41.97	−27.92
N-glycosidic bond	−0.03	11.12
3′,5′-dTDP$^{\bullet-}$		
$C_{5'}$–$O_{5'}$ bond	−32.89	−18.98
$C_{3'}$–$O_{3'}$ bond	−43.09	−27.72
N-glycosidic bond	−7.67	6.57

[a]ΔE = E(Bond-broken product) − E(Radical anion).
[b]ΔE_{PCM} = E(Bond-broken product) − E(Radical anion); using PCM model with ε = 78.39

group. Therefore, this strong interaction would not be expected in real DNA single strands.

The energy release during the N_1–$C_{1'}$ bond breaking process is less significant as compared to that during the C–O σ bond rupture. *N*-glycosidic bond-broken product of cytidine diphosphate ($P_{dCglyco}$) in the gas phase has the total energy almost the same as that of 3′,5′-dCDP$^{\bullet-}$. This bond-ruptured complex contains a dehydrogenated cytosine anion and a phosphate–sugar–phosphate neutral radical in the gas phase. In parallel, the complex formed by the *N*-glycosidic bond breaking of 3′,5′-dTDP$^{\bullet-}$ ($P_{dTglyco}$) is ∼7.67 kcal/mol more stable than 3′,5′-dTDP$^{\bullet-}$. This 7.67 kcal/mol energy release suggests that in the gas phase, the dehydrogenated thymine anion is more stable than the dehydrogenated cytosine anion. Such a phenomenon is in accordance with relatively large electron affinity of the nucleobase thymine.

Inclusion of the polar solvent decreases stability of the *N*-glycosidic bond-broken products compared to the radical anions of the corresponding nucleoside-3′,5′-diphosphates. The total electronic energy of the product of the *N*-glycosidic bond breaking of 3′,5′-dCDP$^{\bullet-}$ ($P_{dCglyco}$) is 11.12 kcal/mol higher than that of 3′,5′-dCDP$^{\bullet-}$. Meanwhile, the PCM model calculations reveal that the total energy of the *N*-glycosidic bond breaking of 3′,5′-dTDP$^{\bullet-}$ ($P_{dTglyco}$) is 6.57 kcal/mol higher than that of 3′,5′-dTDP$^{\bullet-}$. On the other hand, the C–O σ bond rupture products in the polar environment are still significantly more stable than the radical anions of the corresponding nucleoside-3′,5′-diphosphates. The relative energy (relative to the corresponding radical anion) of the $C_{3'}$–$O_{3'}$ bond-broken product of the cytidine diphosphate is −27.92 kcal/mol and that of the thymidine diphosphate is −27.72 kcal/mol. Less significantly, the relative energy (relative to the corresponding radical anion) of the $C_{5'}$–$O_{5'}$ bond-broken product of the cytidine complex is −16.99 kcal/mol and that of the thymidine species amounts to −18.98 kcal/mol. In general, solvent effects increase the energy of the bond-broken products of the pyrimidine diphosphate complexes. It should be noted that this result is contrary to the conclusions of the previous study on the guanosine diphosphate. One concludes that due to the charge relocation to the guanine moiety in aqueous solution, solvent effects

further stabilize the bond-broken products of the guanosine complexes (47).

Both in the gas phase and in the presence of the polarizable medium, the $C_{3'}$–$O_{3'}$ bond breaking process has the highest driving force among the three bond breaking pathways considered in this study. The reaction pathway through the $C_{3'}$–$O_{3'}$ bond breaking is the most thermodynamically favorable. Meanwhile, relatively higher energies of the *N*-glycosidic bond-broken products suggest that the pathway through N_1–$C_{1'}$ bond rupture is not thermodynamically preferred.

Molecular orbital (MO) analysis

An analysis of the singly occupied molecular orbitals (SOMO) provides deeper insights into the electron attachment and the bond breaking mechanisms. Figure 4 illustrates the distribution of the unpaired electron along the LEE-induced bond breaking pathways of the nucleotides. In the gas phase, the characteristics of the SOMOs of 3′,5′-dCDP$^{\bullet-}$ and 3′,5′-dTDP$^{\bullet-}$ indicate that the excess electron is mainly covalent-bonded to the base moiety (Figure 4).

One of the important outcomes of the previous studies on the LEE-induced bond dissociation in the pyrimidine nucleotides is the conclusion that the excess negative charge is partly located on the bond to be broken (13). The SOMO of the transition states in Figure 4 exhibits similar characteristics of the charge-induced bond dissociation.

Consistent with the previous study on the LEE-induced $C_{3'}$–$O_{3'}$ bond breaking in the 3′-dCMP and 3′-dTMP, the excess electron transfer from the base moiety to the anti-bonding orbital of $C_{3'}$–$O_{3'}$ bond through the space can be identified from the SOMO of the corresponding transition state. This electron transfer mechanism accounts for the lower activation energy barrier estimated for the $C_{3'}$–$O_{3'}$ bond dissociation.

The anti-bonding orbital characteristics of the $C_{5'}$–$O_{5'}$ bond are obvious from the SOMO characteristics of the transition state of the $C_{5'}$–$O_{5'}$ σ bond rupture. Similarly, the partial occupation of the *N*-glycosidic anti-bonding MO and partial occupation of the π* orbital of the base moiety is shown in the SOMO of the transition state corresponding to the *N*-glycosidic bond rupture.

The SOMOs of the C–O bond-broken products (Figure 5) confirm that the radical resides on the C5′ of the 2′-deoxypyrimidine-C5′(*HH′*)-yl-3′-monophosphate in $C_{5'}$–$O_{5'}$ σ bond ruptured product and on the C3′ of the 2′-deoxypyrimidine-C3′(*H*)-yl-5′-monophosphate in $C_{3'}$–$O_{3'}$ σ bond-broken product. The characteristics of the SOMOs of the *N*-glycosidic bond dissociation products in gas phase indicate that the radical is located on the C1′ of 2′-deoxyribose-C1′(*H*)-yl-3′,5′-diphosphate.

The solvent effects modify electron distribution. The main influence of the solvent effects on the distribution of the excess electron in the radicals is the increase of the unpaired electron population on the pyrimidine bases. In aqueous solution, the characteristics of the SOMO of the transition state of the $C_{5'}$–$O_{5'}$ σ bond rupture indicate that the excess electron is only slightly shifted to the $C_{5'}$–$O_{5'}$ anti-bonding orbital (Supplementary Data). This phenomenon might be related to the fact that the $C_{5'}$–$O_{5'}$ bond breaking activation energy barrier increases significantly in the PCM model studies. Meanwhile, the SOMO of the transition state of the *N*-glycosidic bond breaking process in the aqueous solution is affected less compared to that in the gas phase. This is directly correlated to the similar activation energy barrier revealed in the aqueous solution and in the gas-phase calculations.

Reaction pathways of the LEE-induced DNA single strands

Based on the electronic affinities and the energy profiles explored in this study, the possible mechanism of the

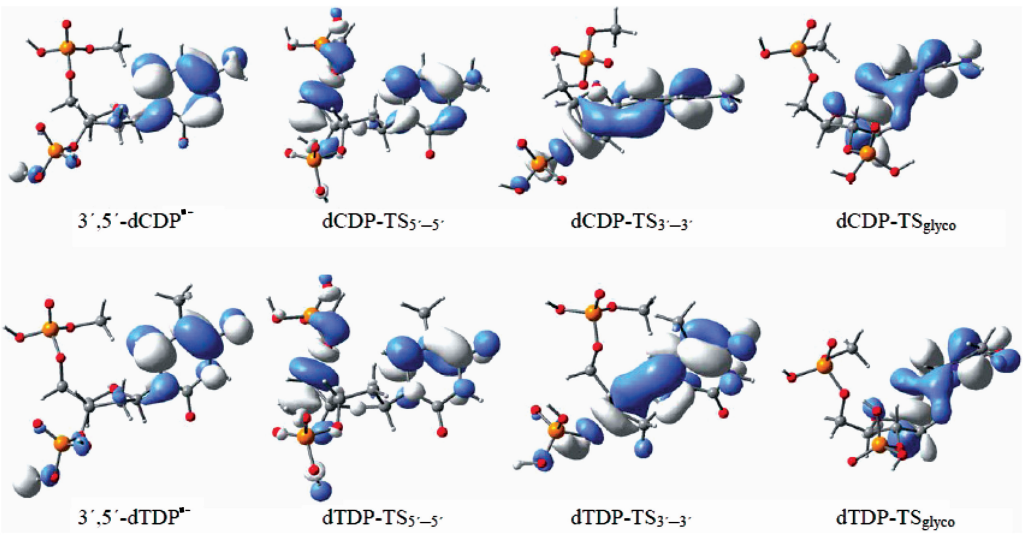

Figure 4. The SOMOs of radical anion of 3′,5′-dCDP$^{\bullet-}$ and 3′,5′-dTDP$^{\bullet-}$, and the corresponding transition states of the $C_{5'}$–$O_{5'}$ bond breaking, $C_{3'}$–$O_{3'}$ bond breaking and *N*-glycosidic bond breaking in the gas phase. The typical characteristics of the σ anti-bond orbital and the breaking bond are shown clearly.

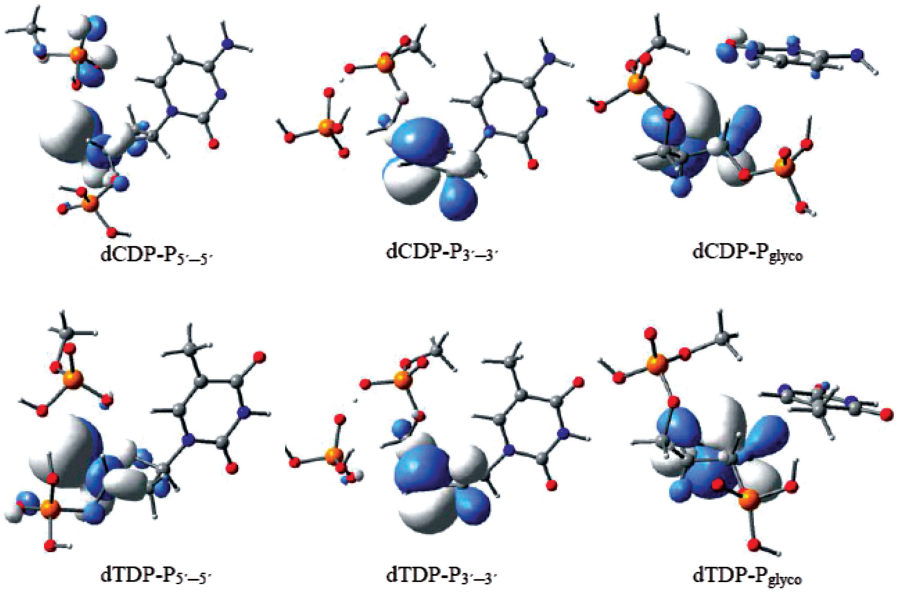

Figure 5. The SOMOs of the bond-broken products in the gas phase.

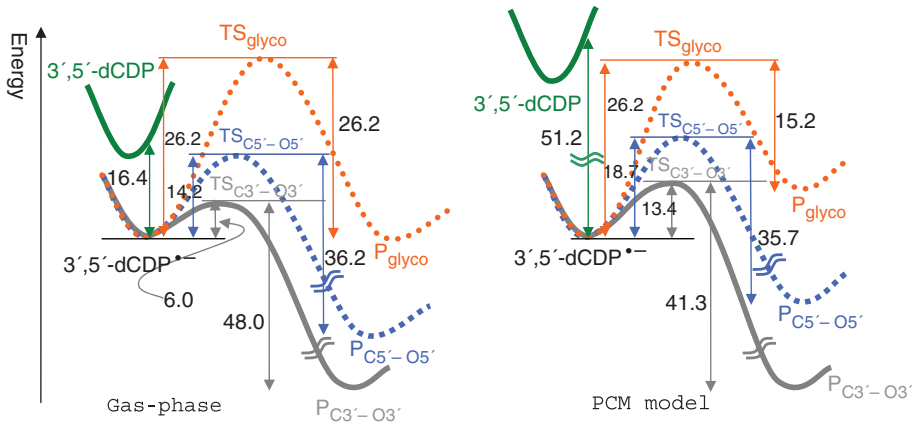

Figure 6. The energy profile of the $C_{5'}$–$O_{5'}$, $C_{3'}$–$O_{3'}$ and *N*-glycosidic bond breaking process for 3′,5′-dCDP$^{\bullet-}$ in the gas phase and in aqueous solutions.

LEE-induced single-strand bond breaking around the pyrimidine sites of the DNA single strands is consistent with the previous mechanism that has been proposed based on the pyrimidine monophosphate models (16,18). That is, the incident electrons bind to the pyrimidine bases in DNA oligomers, forming a base-centered radical anion in the nascent stage. This radical anion is electronically stable enough that either the C–O or glycosidic bond breaking process might compete with the electron detachment and yield corresponding radical fragments and anions.

In the gas phase, the glycosidic bond breaking process requires activation energy as high as 19.19 kcal/mol. Therefore, base release should be excluded based on the mechanisms proposed above. The energy barrier for the $C_{3'}$–$O_{3'}$ σ bond cleavage process (~6.0 kcal/mol for both cytidine and thymidine) suggests that this reaction pathway is the most favorable compared to the other possible pathways. On the other hand, the relatively low activation energy barrier (~14 kcal/mol) for the $C_{5'}$–$O_{5'}$ σ bond cleavage process indicates that this pathway could be possible, especially when the incident electrons have relatively high energy (a few electron volts). However, as the energy of the incident electrons decrease, the possibility of the reactions through the $C_{5'}$–$O_{5'}$ σ bond cleavage pathway is expected to decrease. Therefore, the strand breaks caused by the attachment with near-zero energy electrons is dominated by the $C_{3'}$–$O_{3'}$ σ bond cleavage pathway for the isolated nucleotides.

An application of the PCM model to describe solvent effects excludes accounting for proton transfer or charge transfer processes that might exist between solute and solvent. In this sense, solvent effects greatly increase the activation energies of either C–O σ bond cleavage processes or the *N*-glycosidic bond breaking process. In the solvated condition, the predicted activation energy barriers of 26–28 kcal/mol for the *N*-glycosidic bond

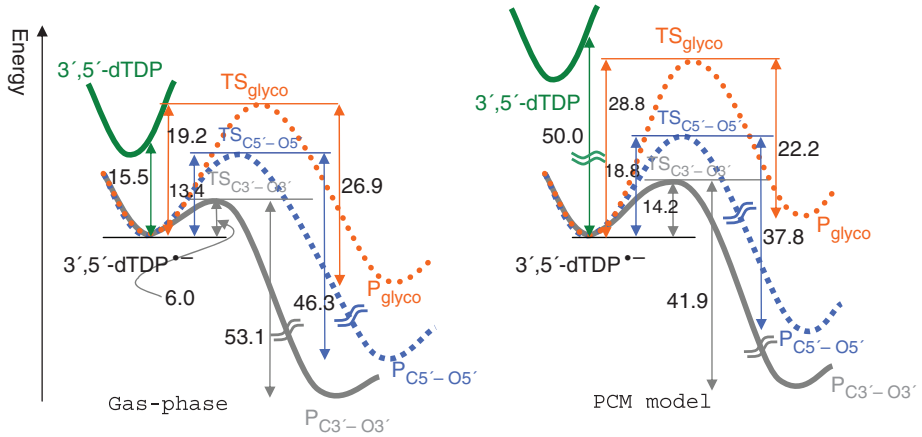

Figure 7. The energy profile of the $C_{5'}$–$O_{5'}$, $C_{3'}$–$O_{3'}$ and *N*-glycosidic bond breaking process for 3′,5′-dTDP$^{\bullet-}$ in the gas phase and in aqueous solutions.

breaking process eliminate possibility of the observable reactions occurring based on this pathway. It is important to note that the activation energy barrier of the $C_{3'}$–$O_{3'}$ σ bond cleavage process rises to 13.4 kcal/mol in the PCM calculations, which is about 5 kcal/mol lower than that for the $C_{5'}$–$O_{5'}$ σ bond cleavage process (18.76 kcal/mol). In comparison with the gas phase, the importance of the $C_{5'}$–$O_{5'}$ σ bond cleavage process (versus the $C_{3'}$–$O_{3'}$ σ bond cleavage process) increases under the solvated condition. However, the $C_{3'}$–$O_{3'}$ σ bond cleavage pathway still dominates the LEE-induced DNA single strands in the presence of the polarizable surroundings. The energy profiles along the reaction pathways depicted in Figures 6 and 7 clearly reveal that the products of the $C_{3'}$–$O_{3'}$ σ bond cleavage are favored both kinetically and thermodynamically. Nevertheless, we want to emphasize again that since the activation energy barriers predicted in the polarizable surroundings are in general higher than those in the gas phase, the LEE-induced DNA single strands breaking in the polarizable medium should be less important than the corresponding phenomenon in the gas phase.

Comparison with the experimental results

It is important to note that the models used in this study represent the pyrimidine sites within the DNA single strands. An addition of the methyl group at the 5′-phosphate group prevents the intramolecular proton transfer from the 5′-phosphate group to the bases (at the C6 of either cytosine or thymine) during the formation of the base-centered radical anions. In fact, without the methylation of the 5′-phosphate group, it is hard to prevent this intramolecular proton transfer during the geometry optimization of the radical anions.

For cytidine, the experiments of LEE-induced bond breaks of oligonucleotide tetramer GCAT in the thin solid films revealed the ratio of 5:11 for the bond breaks of $C_{5'}$–$O_{5'}$ to the bond breaks of $C_{3'}$–$O_{3'}$ (at the site of cytidine) induced by the incident electrons with the energy of 15 eV. This ratio decreases to 3:8 (10 eV) and 4:21 (6 eV) as the energy of the incident electrons diminishes (14). Therefore, one should expect that the ratio of the bond breaks of $C_{5'}$–$O_{5'}$ against that of $C_{3'}$–$O_{3'}$ induced by the near-zero electron attachment will be even smaller. On the other hand, the percentage of the cytosine base release is negligible. This ratio observed in the experiments clearly follows our theoretical sequence of the bond breaking reaction pathways either in the gas phase or in aqueous solutions.

For thymidine, the experiment of LEE-induced bond breaks of oligonucleotide trimer TTT (TpTpT) (29) in the solid films yields the ratio of 2.5:2.9 for the bond breaks of $C_{5'}$–$O_{5'}$ to the bond breaks of $C_{3'}$–$O_{3'}$ with the relatively high-energy incident electrons (11 eV). This ratio is also qualitatively consistent with the theoretical predictions.

Considering that the oligonucleotide GCAT is in the thin solid film in the experiment (14), the influence of the surroundings in the thin solid film on the LEE-induced DNA damages is greater than that in the gas phase but smaller than accounted by the solvent effects modeled by the PCM model. This consistency between the theoretical prediction and the experimental observation in the reaction pathway ratio provides strong supportive evidence for the base-centered radical anion mechanism of the LEE-induced single-strand bond breaking around the pyrimidine sites of the DNA single strands mentioned above.

CONCLUSIONS

One of the possible mechanisms for the LEE-induced single-strand breaking in DNA might involve the electron's attachment to the pyrimidine DNA bases and the formation of the base-centered radical anions of the nucleotides in the first step (9,16,18,19). Subsequently, these electronically stable radical anions are capable of undergoing either C–O or glycosidic bond breaking, producing the neutral ribose radical fragments and the corresponding phosphoric anions or base anions. The results of the present study, along with the findings of the earlier investigations (13,16,18) indicate that this mechanism is able to

elucidate the recent experimental observations on the LEE-induced damages in DNA single strands.

The present results reveal that for the pyrimidine diphosphates in the gas phase, the strand breaks caused by the attachment of near-zero energy electrons is dominated by the $C_{3'}$–$O_{3'}$ σ bond cleavage pathway. The relatively high-activation energy barrier of the $C_{5'}$–$O_{5'}$ σ bond dissociation process suppresses this $C_{5'}$–$O_{5'}$ σ bond rupture pathway. Due to the presence of the adjacent phosphate groups, the high-activation energy barrier for the glycosidic bond breaking suggests that based on the base-centered radical anion mechanism, LEE attachment is unlikely to directly induce the base release at the pyrimidine sites in the DNA single strands.

In the presence of polarizable surroundings, the interactions between the nucleotides and the polarizble medium increase the activation barriers to 13.4 kcal/mol for the $C_{3'}$–$O_{3'}$ bond cleavage and to 18.8 kcal/mol for the $C_{5'}$–$O_{5'}$ bond cleavage. These relatively high-energy barriers ensure either $C_{5'}$–$O_{5'}$ or $C_{3'}$–$O_{3'}$ bond rupture to take place only in a small rate at the pyrimidine sites in DNA single strands. The values of activation energies of these C–O bond cleavages indicate that $C_{3'}$–$O_{3'}$ bond breaking pathway is superior over that of $C_{5'}$–$O_{5'}$. On the other hand, the comparatively high-energy barrier for the *N*-glycosidic bond rupture indicates that this reaction pathway is the least possible.

The good agreement between the ratios for the bond breaks of $C_{5'}$–$O_{5'}$, $C_{3'}$–$O_{3'}$ and *N*-glycosidic bonds observed in the experiment of LEE-induced bond breaks of oligonucleotide tetramer CGAT and trimer TTT in the thin solid films and the theoretical sequence of the bond breaking reaction pathways in the PCM-simulated effects of the polarizable surroundings has been found. This consistency between the theoretical predictions and the experimental observation of the reaction pathway ratio provides strong supportive evidences for the base-centered radical anion mechanism of the LEE-induced single-strand bond breaking around the pyrimidine sites of the DNA single strands.

It should be emphasized that the PCM model only accounts for the effects of the polarizable surroundings. However, there are other important factors governing characteristics of solvated species in aqueous solutions such as microsolvation and proton transfer between solvent and solute, which are not accounted for in the PCM calculations. In addition to the effects of the polarizable surroundings (which increase the activation energy barriers for C–O σ and glycosidic bond cleavage), microhydration and proton transfer between water molecules and the radical anions would further stabilize the reactants by reducing the excessive negative charge of the radical anions. Therefore, electron-induced DNA single-strand bond breaking is not expected to occur in aqueous solutions, as concluded in the experimental studies (48).

SUPPLEMENTARY DATA

Supplementary Data are available at NAR Online.

ACKNOWLEDGEMENT

We would like to thank the Mississippi Center for Supercomputing Research for a generous allotment of computer time.

FUNDING

National Science Foundation (NSF) Centers of Research Excellence in Science and Technology (CREST) (Grant No. HRD-0833178); National Science & Technology Major Project 'Key New Drug Creation and Manufacturing Program', China (Number : 2009ZX09301-001). Funding for open access charge: NSF CREST.

Conflict of interest statement. None declared.

REFERENCES

1. Boudaiffa,B., Cloutier,P., Hunting,D., Huels,M.A. and Sanche,L. (2000) Resonant formation of DNA strand breaks by low-energy (3 to 20 eV) electrons. *Science*, **287**, 1658–1660.
2. Pan,X., Cloutier,P., Hunting,D. and Sanche,L. (2003) Dissociative electron attachment to DNA. *Phys. Rev. Lett.*, **90**, 208102-1–208102-4.
3. Caron,L.G. and Sanche,L. (2003) Low-energy electron diffraction and resonances in DNA and other helical macromolecules. *Phys. Rev. Lett.*, **91**, 113201.
4. Hanel,G., Gstir,B., Denifl,S., Scheier,P., Probst,M., Farizon,B., Farizon,M., Illenberger,E. and Mark,T.D. (2003) Electron attachment to Uracil: effective destruction at subexcitation energies. *Phys. Rev. Lett.*, **90**, 188104-1–188104-4.
5. Zheng,Y., Cloutier,P., Hunting,D., Wagner,J.R. and Sanche,L. (2004) Glycosidic bond cleavage of thymidine by low-energy electrons. *J. Am. Chem. Soc.*, **126**, 1002–1003.
6. Li,X., Sevilla,M.D. and Sanche,L. (2003) Density functional theory studies of electron interaction with DNA: can zero eV electrons induce strand breaks? *J. Am. Chem. Soc.*, **125**, 13668–13669.
7. Huels,M.A., Boudaiffa,B., Cloutier,P., Hunting,D. and Sanche,L. (2003) Single, double, and multiple double strand breaks induced in DNA by 3-100 eV electrons. *J. Am. Chem. Soc.*, **125**, 4467–4477.
8. Abdoul-Carime,H., Gohlke,S., Fischbach,E., Scheike,J. and Illenberger,E. (2004) Thymine excision from DNA by subexcitation electrons. *Chem. Phys. Lett.*, **387**, 267–270.
9. Barrios,R., Skurski,P. and Simons,J. (2002) Mechanism for damage to DNA by low-energy electrons. *J. Phys. Chem. B*, **106**, 7991–7994.
10. Berdys,J., Anusiewicz,I., Skurski,P. and Simons,J. (2004) Damage to model DNA fragments from very low-energy (<1 eV) electrons. *J. Am. Chem. Soc.*, **126**, 6441–6447.
11. Berdys,J., Skurski,P. and Simons,J. (2004) Damage to model DNA fragments by 0.25-1.0 eV electrons attached to a thymine π* orbital. *J. Phys. Chem. B*, **108**, 5800–5805.
12. Berdys,J., Anusiewicz,I., Skurski,P. and Simons,J. (2004) Theoretical study of damage to DNA by 0.2-1.5 eV electrons attached to cytosine. *J. Phys. Chem. A*, **108**, 2999–3005.
13. Gu,J., Xie,Y. and Schaefer,H.F. (2005) Glycosidic bond cleavage of pyrimidine nucleosides by low-energy electrons: a theoretical rationale. *J. Am. Chem. Soc.*, **127**, 1053–1057.
14. Zheng,Y., Cloutier,P., Hunting,D.J., Sanche,L. and Wagner,J.R. (2005) Chemical basis of DNA sugar-phophate cleavage by low-energy electrons. *J. Am. Chem. Soc.*, **127**, 16592–16598.
15. Ray,S.G., Daube,S.S. and Naaman,R. (2006) On the capturing of low-energy electrons by DNA. *Proc. Natl Acad. Sci. USA*, **102**, 15–19.
16. Bao,X., Wang,J., Gu,J. and Leszczynski,J. (2006) DNA strand breaks induced by near-zero-electronvolt electron attachment to

pyrimidine nucleotides. *Proc. Natl Acad. Sci. USA*, **103**, 5658–5663.
17. Zheng,Y., Cloutier,P., Hunting,D.J., Wagner,J.R. and Sanche,L. (2006) Phosphodiester and *N*-glycosidic bond cleavage in DNA induced by 4–15 eV electrons. *J. Chem. Phys.*, **124**, 064710.
18. Gu,J., Wang,J. and Leszczynski,J. (2006) Electron attachment-induced DNA single strand breaks: C-3′-O-3′ sigma-bond breaking of pyrimidine nucleotides predominates. *J. Am. Chem. Soc.*, **128**, 9322–9323.
19. Simons,J. (2006) How do low-energy (0.1-2 eV) electrons cause DNA-strand breaks? *Acc. Chem. Res.*, **39**, 772–779.
20. Sanche,L. (2005) Low energy electron-driven damage in biomolecules. *Eur. Phys. J. D.*, **35**, 367–390.
21. Li,X., Sanche,L. and Sevilla,M.D. (2006) Base release in nucleosides induced by low-energy electrons: a DFT study. *Radiat. Res.*, **165**, 721–729.
22. LaVerne,J.A. and Pimblott,S.M. (1995) Electron energy-loss distributions in solid, dry DNA. *Radiat. Res.*, **141**, 208–215.
23. Kumar,A. and Sevilla,M.D. (2007) Low-energy electron attachment to 5′-thymidine monophosphate: modeling single strand breaks through dissociative electron attachment. *J. Phys. Chem. B*, **111**, 5464–5474.
24. Li,X. and Sevilla,M.D. (2007) DFT treatment of radiation produced radicals in DNA model systems. *Adv. Quantum Chem.*, **52**, 59–87.
25. Schiedt,J., Weinkauf,R., Neumark,D.M. and Schlag,E.W. (1998) Anion spectroscopy of uracil, thymine and amino-oxo and amino-hydrocy tautomers of cytosine and their water clusters. *Chem. Phys.*, **239**, 511–524.
26. Wesolowski,S.S., Leininger,M.L., Pentchev,P.N. and Schaefer,H.F. (2001) Electron affinities of the DNA and RNA bases. *J. Am. Chem. Soc.*, **123**, 4023–4028.
27. Richardson,N.A., Gu,J., Wang,S., Xie,Y. and Schaefer,H.F. (2004) DNA nucleosides and their radical anions: molecular structures and electron affinities. *J. Am. Chem. Soc.*, **126**, 4404–4411.
28. Gu,J., Xie,Y. and Schaefer,H.F. (2006) Near 0 eV electrons attach to nucleotides. *J. Am. Chem. Soc.*, **128**, 1250–1252.
29. Martin,F., Burrow,P.D., Cai,Z., Cloutier,P., Hunting,D. and Sanche,L. (2004) DNA Strand Breaks Induced by 0-4 eV Electrons: the role of shape resonances. *Phys. Rev. Lett.*, **93**, 068101-1–068101-4.
30. Kumar,A. and Sevilla,M.D. (2008) The role of ps* excited states in electron-inducd dna strand break formation: a time-dependent density functional theory study. *J. Am. Chem. Soc.*, **130**, 2130–2131.
31. Kumar,A. and Sevilla,M.D. (2009) Role of excited states in low-energy electron (LEE) induced strand breaks in DNA model systems: influence of aqueous enviroment. *ChemPhysChem.*, **10**, 1426–1430.
32. Li,Z., Zheng,Y., Cloutier,P., Sanche,L. and Wagner,J.R. (2008) Low energy electron induced DNA damage: effects of terminal phosphate and base moieties on the distribution of damage. *J. Am. Chem. Soc.*, **130**, 5612–5613.
33. Gu,J., Xie,Y. and Schaefer,H.F. (2007) Electron attachment to DNA single strands: gas phase and aqueous solution. *Nucleic Acids Res.*, **35**, 5165–5172.
34. Gu,J., Xie,Y. and Schaefer,H.F. (2006) Electron attachment to nucleotides in aqueous solution. *ChemPhysChem*, **7**, 1885–1887.
35. Becke,A.D. (1993) Density-functional thermochemistry 3. The role of exact exchange. *J. Chem. Phys.*, **98**, 5648–5652.
36. Lee,C., Yang,W. and Parr,R.G. (1988) Development of the Colle-Salvetti correlation-energy formula into a functional of the electron-density. *Phys. Rev. B*, **37**, 785–789.
37. Huzinaga,S. (1965) Gaussian-type functions for polyatomic systems. *J. Chem. Phys.*, **42**, 1293–1302.
38. Dunning,T.H. (1970) Gaussian basis functions for use in molecular calculations: 1. Contraction of (9S5P) atomic basis sets for first-row atoms. *J. Chem. Phys.*, **53**, 2823–2833.
39. Dunning,T.H. and Hay,P.J. (1977) In Schaefer,H.F. (ed.), *Modern Theoretical Chemistry*, Vol. 3. Plenum Press, New York, pp. 1–27.
40. Lee,T.J. and Schaefer,H.F. (1985) Systematic study of molecular anion within the self-consistent-field approximation: OH^-, CN^-, C_2H^-, NH_2^-, and CH_3^-. *J. Chem. Phys.*, **83**, 1784–1794.
41. Rienstra-Kiracofe,J.C., Tschumper,G.S., Schaefer,H.F., Nandi,S. and Ellison,G.B. (2002) Atomic and molecular electron affinities: photoelectron experiments and theoretical computations. *Chem. Rev.*, **102**, 231–282.
42. Stokes,S.T., Li,X., Grubisic,A., Ko,Y.J. and Bowen,K.H. (2007) Intrinsic electrophilic properties of nucleosides: photoelectron spectroscopy of their parent anions. *J. Chem. Phys.*, **127**, 084321–084326.
43. Cossi,M., Barone,V., Cammi,R. and Tomasi,J. (1996) Ab initio study of solvated molecules: a new implementation of the polarizable continuum model. *Chem. Phys. Lett.*, **255**, 327–335.
44. Reed,A.E. and Schleyer,P.R. (1990) Chemical bonding in hypervalent molecules. The dominance of ionic bonding and negative hyperconjugation over d-orbital participation. *J. Am. Chem. Soc.*, **112**, 1434–1445.
45. Reed,A.E., Curtiss,L.A. and Weinhold,F. (1988) Intermolecular interactions from a natural bond orbital, donor-acceptor viewpoint. *Chem. Rev.*, **88**, 899–926.
46. Frisch,M.J., Trucks,G.W., Schlegel,H.B., Scuseria,G.E., Robb,M.A., Cheeseman,J.R., Montgomery,J.A. Jr, Vreven,T., Kudin,K.N., Burant,J.C. *et al.* (2003) *Gaussian 03*. Revision C.02. Gaussian, Inc., Pittsburgh, PA.
47. Gu,J., Wang,J. and Leszczynski,J. (2010) Comprehensive analysis of the DNA strand breaks at the guanosine site induced by low energy electron attachment. *ChemPhysChem.*, **11**, 175–181.
48. von Sonntag,C. (2007) Free-radical-induced DNA damages as approached by quantum-mechanical and Monte Carlo calculations: an overview from the standpoint of an experimentalist. *Adv. Quantum Chem.*, **52**, 5–20.